



OPEN

SUBJECT AREAS:
CHEMICAL TOOLS
PREDICTIVE MARKERSReceived
9 July 2014Accepted
9 September 2014Published
1 October 2014Correspondence and
requests for materials
should be addressed to
J.C.W. (jcwu@ecust.
edu.cn) or H.T.
(tianhe@ecust.edu.cn)* These authors
contributed equally to
this work.

A peptide probe for the detection of neurokinin-1 receptor by disaggregation enhanced fluorescence and magnetic resonance signals

Jingxian Wu^{1*}, Rongfeng Zou^{1*}, Qi Wang², Yajing Xue³, Ping Wei⁴, Shiping Yang⁵, Junchen Wu¹ & He Tian¹

¹Key Laboratory for Advanced Materials and Institute of Fine Chemicals Institution, East China University of Science and Technology, Meilong Road 130, Shanghai 200237, China, ²College of Public Health, Nantong University, Seyuan Road 9, Nantong, Jiangsu 226019, China, ³Clinical laboratory, Nantong Tumor Hospital, West Qingnian Road 48, Nantong, Jiangsu 226006, China, ⁴Cancer Institutes, Fudan University Shanghai Cancer Center, Dongan Road 270, Shanghai 200032, China, ⁵Department of chemistry, Shanghai Normal University, Guilin Road 100, Shanghai 200234, China.

We report a novel peptide probe for the detection of neurokinin-1 receptor using disaggregation-caused signal enhancement. The probe was obtained via the aggregation of a modified substance P in a terpyridine-Fe (II) complex with Gd (III)-DOTA into well-defined nanostructures, which effectively weaken ligand fluorescence and slow the exchange rate of inner-sphere water molecules. This probe disaggregates upon binding to the neurokinin-1 receptor and activates the contrast agents to generate a fluorescent signal that positively enhances magnetic resonance imaging contrast and allows for the detection of overexpressed receptors on tumor cells and the identification of lung cancer using serum samples.

Neurokinin-1 receptor (NK1R), a member of the tachykinin family of G-protein coupled receptors (GPCRs), is overexpressed and secreted mainly by breast, ovarian, prostate, lung, thyroid, and glioblastoma tumors^{1,2}. NK1R is widely distributed in the lungs in various cell types, including endothelial, epithelial, and smooth muscle cells; monocytes; macrophages; neutrophils; fibroblasts; and mast cells³. NK1R facilitates the survival, proliferation, and metastasis of cancer cells in tissues and blood^{4,5}. Moreover, human normal cells express NK1R, although the expression levels are much lower compared to cancer cells⁶⁻⁸. Therefore, the tracking and detection of NK1R as a potential biomarker may yield important biological information for the study of cancer, especially lung cancer patients treated with “personalized medicine”^{9,10}. Strategies for the clinical detection of lung cancer include molecular imaging, endoscopy, biopsy and blood biochemical tests, but the mortality of lung cancer patients remains high¹¹⁻¹⁴. In this context, we reasoned that molecular probes may be a powerful tool with which to address the urgent need for early clinical diagnosis and therapy.

A large number of magnetic resonance imaging (MRI) and fluorescence imaging (FI) probes have been developed to sense biomedical-related species, such as nucleic acids¹⁵⁻¹⁷, sugars^{18,19}, enzymes^{20,21}, and specific proteins on cell surfaces²²⁻²⁵, which further improves the accuracy of disease detection. For example, molecular beacons of nucleic acid aptamers have been used to track mRNA in living cells and efficiently isolate cancer cells from blood^{26,27}. In addition, MRI is a noninvasive imaging modality that plays a vital role in the detection of cell surface biomarkers using Gd (III)-DOTA complexes²⁸⁻³⁰. Surprisingly, there are no reports of a dual-modal probe for both FI and MRI for the identification of lung cancer based on disaggregation-caused signal enhancement. This type of probe exhibits the following distinct advantages³¹: 1) the initial signal from ligands is markedly weakened by aggregation, 2) the probe signal is restored or enhanced by disaggregation upon binding to targets, and 3) the probe can be used to obtain images of high spatial and temporal resolution and provide synergy for the clinical identification of diseases. We report a disaggregation-based probe for use in FI and MRI that selectively binds to NK1R *in vitro* by tailoring the neuropeptide substance P (SP; sequence, RPKPQQFFGLM-NH₂, a known ligand of NK1R; Figure 1A), which has the potential for use in lung cancer diagnosis³²⁻³⁴.

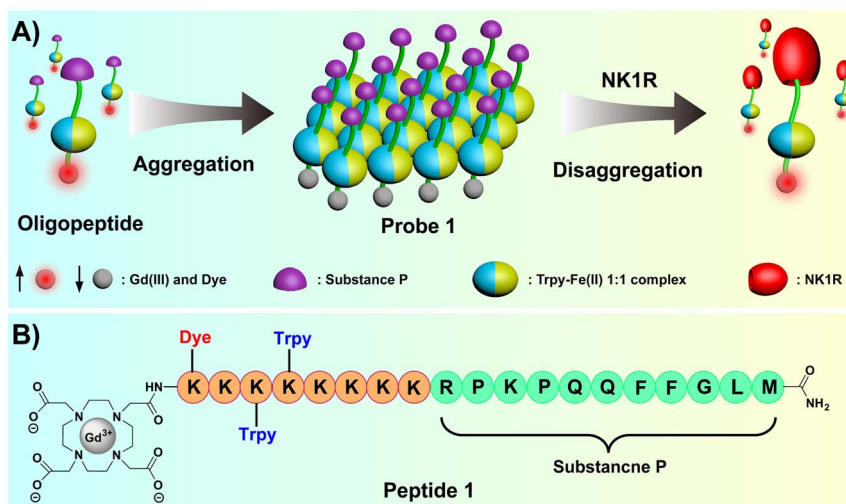


Figure 1 | (A) Schematic representation of the disaggregation-caused signal enhancement. (B) Structure of the peptide Gd(III)-DOTA complex.

Results

Synthesis and formation of probe 1. The probe in this study utilizes the original SP sequence as the binding head group, and eight lysine residues are attached with two terpyridines and a fluorophore (hemicyanine dye) to construct a binary complex with Fe(II) ions for monitoring NK1R levels in cancer cells^{35,36}. Gd(III)-DOTA is connected to the N-terminus as a contrast agent to generate MRI signals. Peptide 1 was synthesized on Rink amide resin using an Fmoc solid-phase method (Figure 1B) and purified to 99.0% purity with a yield of 8.2% after cleavage and deprotection. The formation of peptide 1 and the Gd(III) complex was confirmed using MALDI-TOF (see Supporting Information [SI] for details).

Subsequently, the formation of the terpyridine-Fe(II)-Gd(III)-DOTA complex was monitored using UV/Vis and fluorescence spectra. New absorption peaks appeared at approximately 330 and 530 nm after the addition of Fe(II) ions to a TBS solution of peptide 1 (Figure S1A). Concomitantly, fluorescence at 610 nm decreased until the molar ratio of Fe(II) to peptide 1 reached 1:1 (Figure S1B). Furthermore, the equivalence point shown in Figure S1C clearly indicates the formation of a terpyridine-Fe(II) complex at a ratio of 1:1 ($K_d = 0.35 \mu\text{M}$, Figure S1D). Probe fluorescence was obviously weakened with complex aggregation and the subsequent aggregation of hemicyanine dye via an aggregation-caused quenching (ACQ) effect^{37,38}. Gel electrophoresis experiments identified that the molecular weight of the complex probe 1 was approximately 16.7–26.9 kDa, which suggests it had a polymerization degree (n) of approximately four to six (Figure S3). Moreover, the fluorescence of terpyridine-Fe(II) complex probe was restored most likely because of complex disaggregation under electrophoresis conditions. Fluorescence assays were performed under different pH values (4–8) and temperature (25–50°C) conditions to reveal the stability of probe 1. No significant changes were observed for the fluorescence intensity of probe 1 (Figure S2). Taken together, these results further confirmed that the complex probe exhibited good stability for *in vitro* diagnosis³⁹.

The formation mechanism of probe 1. The formation of probe 1 was characterized using transmission electron microscopy (TEM) to gain insight into the aggregation and disaggregation process of the probe. Peptide 1 itself aggregated into a threadlike network of nanofibers with diameters of approximately 3.5 nm and lengths of several hundred nm in TBS solution (Figure 2A). In contrast, probe 1 (containing the terpyridine-Fe(II)) itself aggregated into a transparent thin film (Figure 2B). NK1R multimers had diameters of approximately 3.8 nm (Figure 2D). The expression of NK1R is

shown in Figure S4. Probe 1 started to disaggregate into different nanofibers with a diameter of approximately 7.5 nm and length of 200–500 nm upon binding to NK1R (Figure 2C). Interestingly, the diameter of these fibers was approximately the sum of those of the peptide 1 and NK1R fibers. The aggregation and disaggregation process of probe 1 was also tracked using DLS. The volume sizes of probe 1 (approximately 1860 nm) were obviously larger than peptide 1 (approximately 2.9 nm) upon the addition of Fe(II) ions (1.0 eq.) to a TBS solution of peptide 1 (Figure S6). In contrast, the volume sizes of probe 1 were changed from approximately 1860 nm to approximately 5.9 nm upon addition of NK1R (1.0 eq.) to a TBS solution of probe 1, which is consistent with TEM. We then determined the binding dissociation constant of probe 1 for NK1R in TBS ($K_d = 2.3 \mu\text{M} > 0.35 \mu\text{M}$) using fluorescence polarization to determine whether the disaggregation of probe 1 broke down the terpyridine-Fe(II) complex (Figure S5)⁴⁰. The results showed that probe 1 remained highly stable after binding with NK1R.

Tracking the levels and localization of NK1R *in vitro*. We used our stable probe 1 to determine whether the fluorescent and magnetic signals of probe 1 changed upon binding to NK1R in cells and tissues. The fluorescence intensity of probe 1 increased by approximately 3-fold at 610 nm upon binding to an equivalent amount of NK1R in TBS (Figure 3A). The binding interaction between ligand and receptor increased fluorescence, which could be used to detect NK1R overexpression in human pulmonary carcinoma A549 cells. The amount of cellular uptake of probe 1 and NK1R overexpression in A549 cells were quantitatively evaluated using flow cytometry⁴¹. Normal human bronchial epithelial (HBE) cells were used as a negative control. Figures 3B and S7 illustrate the significant differences in fluorescence intensity between A549 and HBE cells after incubation with probe 1 at concentrations of 0.5–20 μM in 1640 media. The fold increases in mean fluorescence intensity (MFI) values between A549 and HBE cells reached approximately 6.0-fold at 0.5 μM but only approximately 2.5-fold at 20.0 μM , and the fold increases in MFI values between A549 and HBE cells changed markedly with changes in probe 1 concentration from 2.0 to 20.0 μM ⁴². These results demonstrate that probe 1 is taken up by A549 cells as a result of the overexpression of NK1R.

Confocal laser scanning microscopy (CLSM) was used to track NK1R in HBE and A549 cells to confirm the cellular localization of NK1R. A colocalization experiment of probe 1 with DAPI (the nuclear counter stain) was performed. Blue and red signals in cell images were from DAPI (Figure 3C and 3F) and probe 1 (Figure 3D and 3G), respectively. The overlay images demonstrated that probe 1

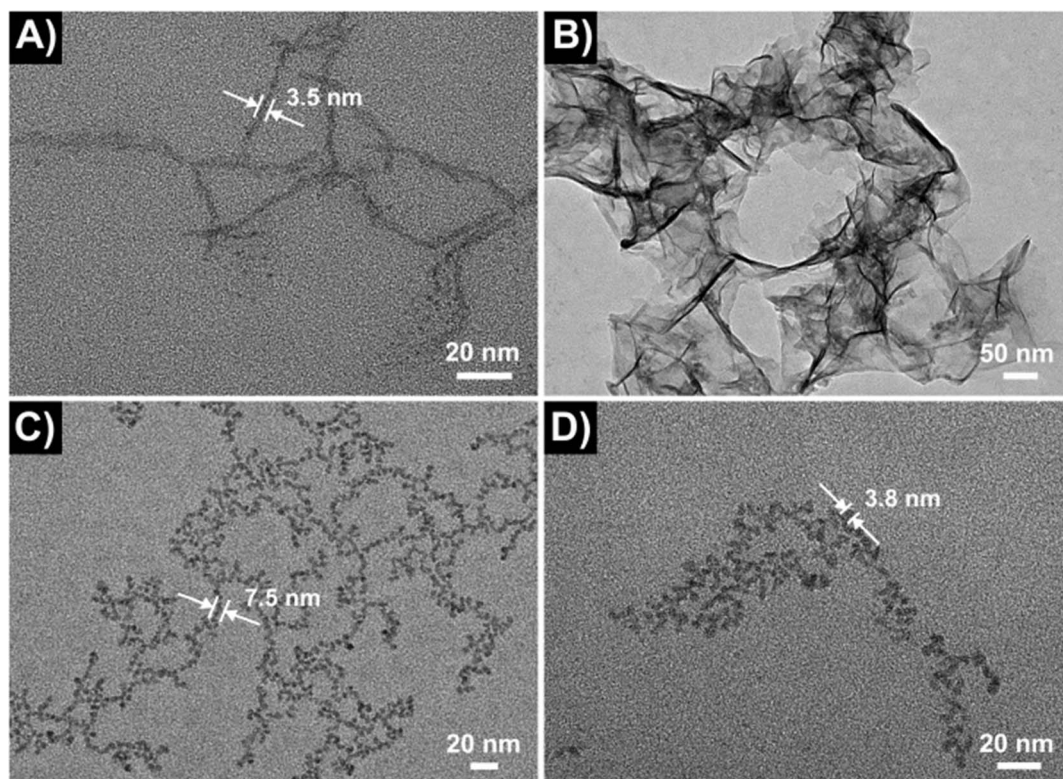


Figure 2 | TEM images: (A) Peptide 1 (10.0 μM). (B) Probe 1 (10.0 μM). (C) Probe 1 bound to NK1R (molar ratio = 1 : 1). (D) NK1Rs (1.0 μM) were stained with sodium phosphotungstate (2.0 wt% aqueous solution) in TBS (pH 7.4, 50.0 mM Tris, 50.0 mM NaCl).

accumulated in the cytoplasm and membrane of A549 (Figure 3E) and HBE (Figure 3H) cells. In addition, probe 1 rapidly distributed in 3.0–5.0 μm lung cancer tissue slices (Figure S8), which is consistent with the results of CLSM and flow cytometry. These results confirmed that probe 1 specifically targeted NK1R. Additionally, the effect of probe 1 on cell proliferation was measured using an MTT assay to determine the cytotoxicity of probe 1. These results indicated that the viability of A549 cells was over 70% after a 24 h incubation with 0–40 μM of probe 1, which indicates a low cytotoxicity of probe 1 (Figure S9).

Detection of NK1R levels using MRI. The relaxivity of probe 1 was measured in TBS using a 0.5 T MR system to validate the T_1 -weighted contrast ability (Figure 4A). The r_1 of probe 1 was determined to be $34.9 \text{ mM}^{-1}\text{s}^{-1}$, which is approximately 3-fold greater than that of peptide 1 ($r_1 = 11.8 \text{ mM}^{-1}\text{s}^{-1}$). The relatively high relaxivity was mainly attributed to the formation of four to six efficiently relaxing Gd (III) centers within a rigid supramolecular structure (high density of relaxivity)^{43–45}. Moreover, the relaxivity of probe 1 was higher than those of the clinical contrast agents Gd-(DTPA) ($r_1 = 4.6 \text{ mM}^{-1}\text{s}^{-1}$) and Gd-(HP-DO3A) ($r_1 = 4.3 \text{ mM}^{-1}\text{s}^{-1}$) under the same conditions^{46,47}. We then tested the T_1 relaxation rates of probe 1 at a fixed concentration (20 μM) in a series of NK1R solutions. Increasing amounts of NK1R triggered an increased disaggregation of probe 1 with a corresponding enhancement in T_1 relaxation rates until the molar ratio of probe 1 : NK1R reached 1 : 1 (Figure 4B). The insert image in Figure 4B shows an obvious change in signal intensity between T_1 -weighted images under molar ratios of 1 : 10 and 1 : 1 (NK1R : probe 1). These results indicated that the enhancement of T_1 relaxation rates of probe 1 was due to the environmental changes in Gd (III)-DOTA from relative hydrophobicity to hydrophilicity after binding to the ligand-binding pocket of NK1R, which further increased the exchange rate

of inner-sphere water molecules [for details, see Equations (1–6) in the Methods section].

Fifteen serum samples were taken from patients and healthy control subjects to test the sensitivity and specificity of probe 1 for NK1R in lung cancer cases. The samples were treated with probe 1, and T_1 and fluorescence signals were determined. The results are summarized in Figures 5 and S10 and Table S1 and indicated no significant difference in the fluorescence signal of probe 1 between serum samples from lung cancer patients and healthy controls. However, the T_1 values for lung cancer serum samples were below 810 ms with the addition of probe 1, and the observed values reached as low as 710 ms in some cases (controls were approximately 950 ms). However, the T_1 values for healthy control sera were approximately 850 ms, with no samples below 810 ms (controls were approximately 950 ms). Therefore, the T_1 values of serum samples treated with probe 1 from healthy individuals were significantly higher than the samples treated with probe 1 from lung cancer patients, and a cutoff value of 810 ms may provide an experimental basis for evaluating whether a patient is suffering from lung cancer. In agreement with Figure 4B, the signals of probe 1 (Figure 5) were enhanced upon binding to NK1R. Accordingly, the concentration of NK1R in sera from lung cancer patients was higher than in sera of individuals without lung cancer⁴⁸. These results also suggested that MRI may be superior to optical bioimaging in the diagnosis of complicated systems⁴⁹.

Discussion

In conclusion, a proof-of-concept for the creation of a fairly efficient activatable MRI contrast agent and fluorescence imaging of probe 1, which is sensitive for the detection of NK1R, is reported. The aggregation of the probe 1 complex containing four to six terpyridine-Fe (II) and Gd (III)-DOTA enabled a slowing of the exchange rate of inner-sphere water molecules. Moreover, the fluorescence of

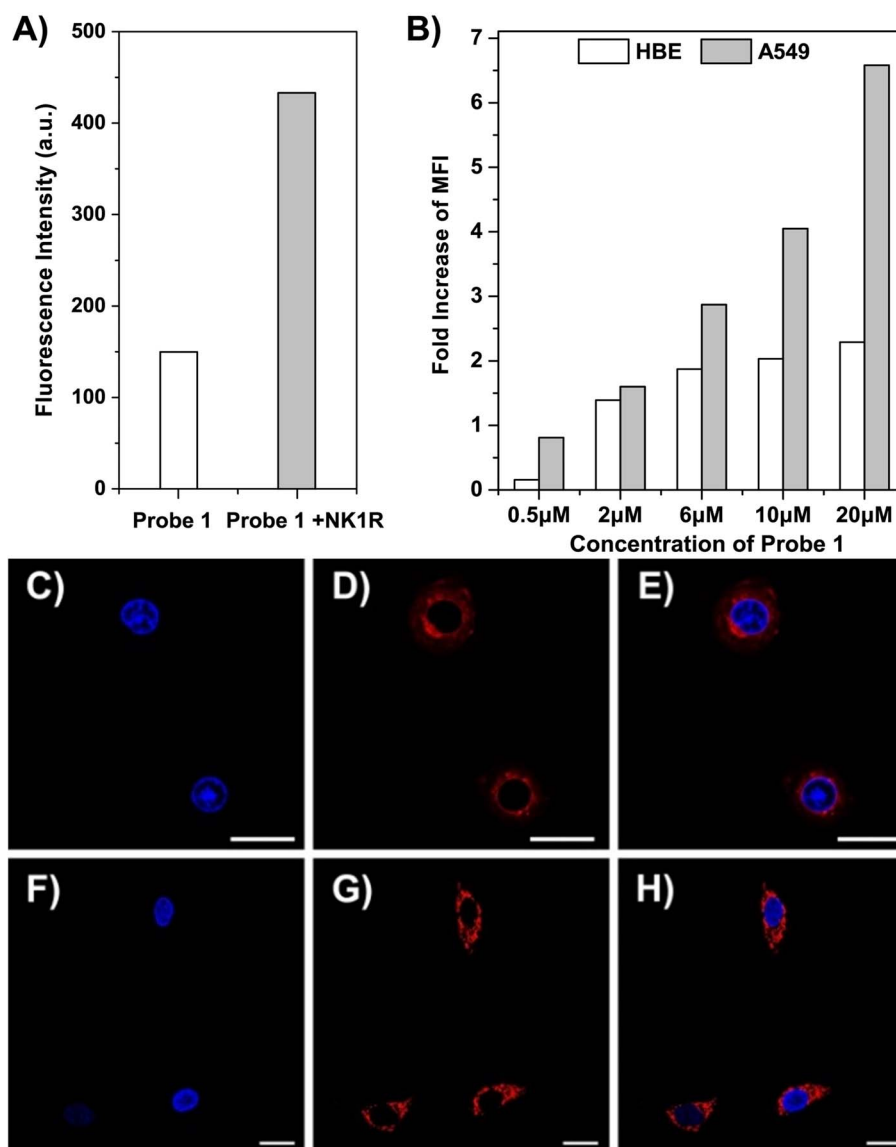


Figure 3 | (A) The fluorescence of 10 μM probe 1 ($\lambda_{ex} = 540$ nm, $\lambda_{em} = 610$ nm) was markedly increased upon the addition of equal amounts of NK1R in TBS (pH 7.4, 50.0 mM Tris, 50.0 mM NaCl). (B) The fold-increase values of MFI of A549 (gray) and HBE (blank) cells treated with different concentrations of probe 1 (0.5–20 μM) in 1640 media. (C)–(H) CLSM images of HBE (C–E) and A549 (F–H) cells treated with 10 μg/mL DAPI (C and F) and 10 μM probe 1 (D and G); (E) overlay of (C) and (D); and (H) overlay of (F) and (G). (Scale bar, 20 μm).

probe 1 itself was effectively weakened by an aggregation-caused quenching (ACQ) effect. Positive MRI contrast enhancement was activated after binding to NK1R, which triggered the disaggregation of probe 1 by increasing the exchange rate of water molecules between inner- and out-spheres. The fluorescence of probe 1 was restored by increases in the distance between the dyes. We demonstrated that this concept can be used to monitor levels of NK1R in cancer cells and distinguish lung cancer patients from healthy individuals using a serum assay. Further studies on probe 1 are underway in our laboratory.

Methods

Synthesis of the peptide 1. The peptide was synthesized using a Microwave Peptide Synthesizer (CEM, USA) on Rink amide resin. The resin (312 mg, 0.8 mmol/g, 0.25 mmol, 1.0 equiv.) was weighed into plastic peptide synthesis vessels and allowed to swell in DMF (10.0 mL) for 1.5 h. An intensive cycle with DMF and the following 18 amino acids were attached under microwave radio conditions using the standard solid-phase peptide synthesis method: Fmoc-Met-OH (0.75 mmol, 3.0 equiv.), PyBOP (0.75 mmol, 3.0 equiv.) and DIPEA (1.5 mmol, 6 equiv.) in DMF (10.0 mL). The Fmoc protection group was removed by agitation with piperidine (20%) in DMF

under microwave radio conditions. After the Fmoc-Lys(Alloc)-OH was coupled, the Alloc group was removed by the addition of Pd(PPh₃)₄ (0.05 mmol, 0.2 equiv.) and PhSiH₃ (12 mmol, 48 equiv.) in DCM under argon for 30 min, and terpyridine (1.5 mmol, 6.0 equiv.) and 2-(4,7,10-tris(2-(tert-butoxy)-2-oxoethyl)-1,4,7,10-tetraazacyclodecan-1-yl) acetic acid (0.75 mmol, 3.0 equiv.) were coupled at room temperature. The product was cleaved from resin by TFA/H₂O/Tis (95:2.5:2.5) for 3 h. After removing TFA, the peptides were precipitated three times using diethyl ether and centrifuged at 10,000 rpm for 10 min. The crude peptides were purified using HPLC on an RP18-column using water/CH₃CN (with 0.05% TFA) as the eluent. The solid was dissolved in water (20 mL), acidified with hydrochloric acid (0.1 N, 5 mL) and lyophilized. This step was repeated three times. The product was identified using MALDI-TOF.

Synthesis of peptide 1 complex. The complex of the ligand with Gd (III)-ion was performed using the dropwise addition of an aqueous solution of GdCl₃ to an aqueous solution of the ligand at pH 3.0. The mixture was stirred for 6 h, and the pH was adjusted to 6.5 using a 1 M solution of NaOH. The final Gd (III)-peptide 1 complex was obtained as a purple powder after lyophilization (the excess of GdCl₃ was dialyzed in MilliQ water). The formation of the complex was identified using MALDI-TOF.

Synthesis of probe 1. The complex of the ligand with Fe (II)-ion was performed using the dropwise addition of an aqueous solution of FeCl₂ to an aqueous solution of Gd (III)-DOTA peptide 1. The mixture was stirred at room temperature for 6 h, and the

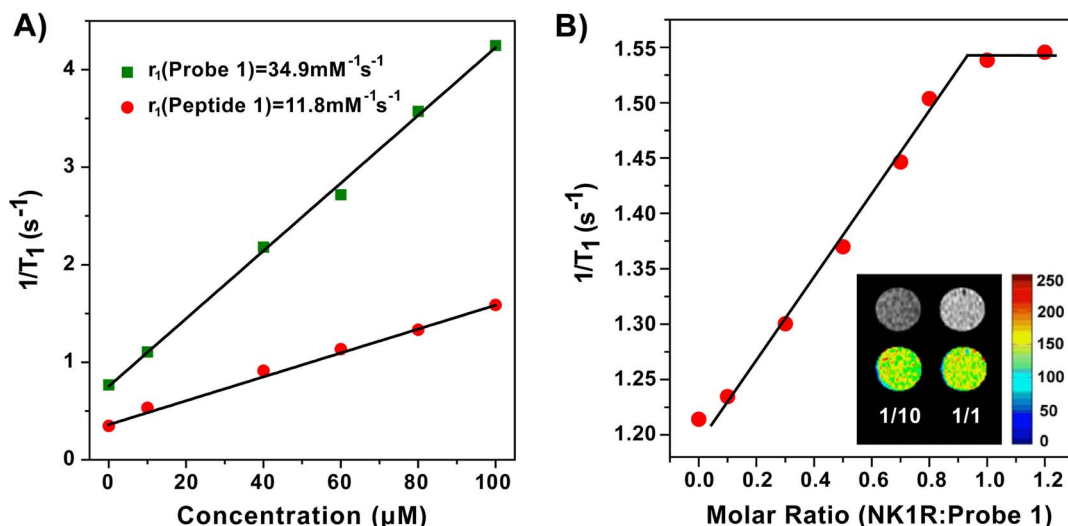


Figure 4 | (A) T₁ relaxation rates ($1/T_1$) of peptide 1 and probe 1 at different concentrations in TBS (pH 7.4, 50.0 mM Tris, 50.0 mM NaCl, 37°C) in the 0.5 T MR system. The slope indicates the r_1 . Differences at starting points were due to the use of different batches of TBS in the experiments.

(B) The dependence of the relaxation rate ($1/T_1$) of probe 1 (20 µM) on the concentrations of NK1R in TBS (pH 7.4, 50.0 mM Tris, 50.0 mM NaCl, 37°C). Inset: T₁-weighted images at the molar ratios of 1 : 10 and 1 : 1 (NK1R : probe 1).

pH was adjusted to 7.0 using a 1 M solution of NaOH. The final probe 1 was obtained as a purple powder after lyophilization (the excess of FeCl₂ was dialyzed in MilliQ water).

Fluorescence and absorption experiments. General procedures: All absorption and fluorescence spectra were recorded using a Varian Cary 100 Conc UV-Visible Spectrometer and a Varian Cary Eclipse Fluorescence Spectrometer at room temperature. Each sample was excited at a wavelength that was appropriate for the fluorescent peptide. The slit widths were set to 5 nm for excitation and emission. Data points were collected at 1 nm increments with a 0.1 s integration period. All spectra were corrected for intensity using the manufacturer-supplied correction factors and corrected for background fluorescence and absorption by subtracting a blank scan of the buffer system.

Gel electrophoresis. Gel electrophoresis was accomplished using a Mini-Vertical gel electrophoresis unit (GE, USA). Samples were treated with loading buffer containing 10 mM Tris (pH 8.5), 20% (v/v) glycerol, and 1% SDS (w/v). Commercially available markers (Hualan, China) were applied for the calculation of apparent molecular weights. Electrophoresis was performed in polyacrylamide mini-gels (1 mm thick) using a discontinuous buffer system. The separation gel (pH 8.8) contained 12% polyacrylamide. The stacking gel (pH 6.8) contained 5% polyacrylamide. Both gels

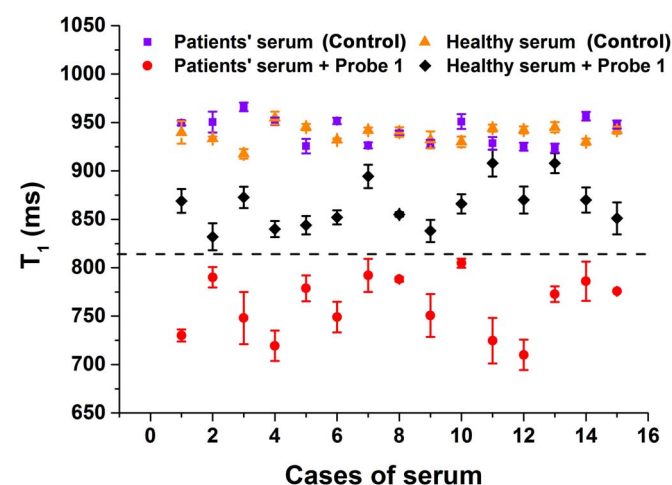


Figure 5 | Clinical detection of NK1R using the 0.5 T MR system. Serum samples collected from 15 patients (control) and 15 healthy individuals (control) were measured in the presence and absence of probe 1 (20 µM) in TBS (pH 7.4, 50.0 mM Tris, 50.0 mM NaCl, 37°C), and T₁ was determined. Means ± SD (n = 3), *P < 0.001.

had an acrylamide/bis ratio of 29 : 1. The running buffer contained 25 mM Tris (pH 8.4), 250 mM glycine and 0.1% SDS (w/v) in water. All solutions were freshly prepared prior to use. SDS-PAGE was performed on a vertical polyacrylamide gel system at 75 V for 3 h. The results were analyzed using Image Quant LAS 4000 (GE, USA).

NK1R expression and purification. Protein expression was induced with IPTG in a liquid LB media with Amp in Rosetta (DE3) overnight at 28°C and purified using nickel affinity chromatography. The concentration of the NK1R solution was determined using the Bradford method and a BSA standard curve. Protein identity was confirmed using NK1R samples dissolved in 50 mM TBS with a final concentration 0.928 mg/mL for analysis. Plasmid pET-21a provided with TACR1(NCBI:NM-015727.27) was transformed into the host of Rosetta (DE3), and recombinant clones were screened using the solid medium of LB with Amp. A single recombinant clone of Rosetta-TACR was selected from solid LB medium with Amp and added to 4 mL fluid medium for culture overnight with shaking at 200 rpm. A total of 5 mL fresh fluid medium in four tubes was prepared and used in a 100 : 1 proportion compared with the overnight cultured fluid medium for recombinant clones to grow to a logarithmic phase (OD₆₀₀ ≈ 0.5) at 37°C. IPTG was added to a final concentration of 1 mM to three tubes, and clones were cultured in 37°C, 28°C and 16°C. The fourth tube at 37°C served as a control. All fluid media had Amp added. When OD₆₀₀ reached 1.5, the cells were collected and ultrasonically disrupted. Supernatants and precipitates were collected. SDS-PAGE electrophoresis determined whether the target protein was expressed in supernatants or precipitates. Recombinant bacteria were inoculated to 4 mL liquid LB media and activated overnight. The media mixture described above was transferred into fresh 400 mL liquid LB medium in a conical flask. Bacteria were treated with IPTG at a final concentration of 1 mM in the logarithmic phase, and overnight induction was performed. The induced bacteria were collected through centrifugation of the LB medium and disrupted by ultrasound. The supernatant was chosen using nickel ion metal affinity chromatography to purify the target protein.

Determination of binding dissociation constant. Fluorescence polarization was used to determine the dissociation constant. Probe 1 (3.0 nM) in TBS (pH = 7.4, 50.0 mM Tris, 50.0 mM NaCl) and different concentrations of NK1R varying from 15 nM–80 µM were added to black, non-treated 96-well plates (Costar). The FP signal was measured after culturing for two h using a Synergy H4 Hybrid Microplate reader (BioTek, USA) with an excitation wavelength at 540 nm and an emission wavelength at 620 nm. Dissociation constants (K_d) between probe 1 and NK1R were determined using non-linear least squares analysis.

Transmission electron microscopy (TEM). High-resolution images of peptide 1, probe 1 and NK1R were acquired using TEM. Samples of peptide 1, probe 1 and the complex of probe 1 and NK1R were prepared by placing a few droplets onto a carbon-coated grid with holes. Samples of NK1R were stained with sodium phosphotungstate (2.0 wt% aqueous solution) and dried at room temperature for 12 h. TEM characterization was performed using a JEM-2100 electron microscope (JEOL, Japan).

Dynamic light scattering (DLS). All DLS experiments were performed on a Malvern Instruments Zetasizer Nano ZS at 37°C, and starting solutions were filtered prior to



use. Samples of peptide 1, probe 1, NK1R and complex of probe 1-NK1R were prepared in TBS (pH 7.4, 50 mM Tris, 50 mM NaCl) in a total sample volume of 1.0 mL.

Flow cytometric assay. Cells were cultured in RPMI 1640 medium (Gibco) supplemented with 10% fetal bovine serum, 100 U penicillin and 0.1 mg of streptomycin (Hyclone) per mL at 37°C with 5% CO₂.

The quantitative evaluation of cellular uptake was performed using flow cytometry (BD FACS Aria). A549 cells and HBE cells were seeded in 6-well plates (10⁶ cells/well) and cultured in 1640 (1 mL) containing 10% FBS for 12 h. Probe 1 dispersed in 1640 medium (1 mL) with different concentrations from 0.5 μM to 20 μM was added, and the cells were incubated at 37°C for 15 min. The medium was removed, and the cells were washed three times with phosphate-buffered saline (PBS). Then, the cells were digested using trypsin and collected in centrifuge tubes via centrifugation at 1000 rpm for 5 min. The supernatant was discarded, and PBS was added to suspend the cells. Suspended cells were examined using flow cytometry. Cells untreated with probe 1 were used as negative controls. The fluorescence scan was performed with 1 × 10⁴ cells. The fold increases in values of mean fluorescence intensity (MFI) were calculated using the following equation: The fold-increased values of MFI = (MFI of treatment group - MFI of control)/MFI of control.

Staining of tissue slices. Tissue slices from lung cancer patients were deparaffinized in xylene and incubated in 96% ethanol. Endogenous peroxidase activity was blocked by incubating the slices in methanol with 1.5% H₂O₂ for 10 min. For antigen retrieval, the sections were boiled in citrate buffer (2.94 g/L sodium citrate, pH 6.0) for 10 min and subsequently cooled to room temperature. After washing with PBS, slices were incubated with 20 μM probe 1 for 12 h at 4°C. Then, the slices were washed three times with PBS and mounted in DAPI (10 μg/mL). Confocal laser scanning microscopy was used for tissue imaging.

MTT assay. All cell lines were purchased from Shanghai Bogoo Biotech Co., Ltd., China. Cytotoxicity was measured using the 3-(4, 5-dimethylthiazol-2-yl)-2, 5-diphenyltetrazolium bromide (MTT) assay in an A549 cell line. Cells growing in the log phase were seeded into 96-well cell-culture plates at 5 × 10⁴/well. The cells were incubated for 12 h at 37°C in 5% CO₂. Solutions of probe 1 (100.0 μL/well) at concentrations of 10, 20, 30, 40 μM in RPMI 1640 were added to wells of the treatment group, and 100.0 μL of RPMI 1640 was added for the negative control group. The cells were incubated for 24 h at 37°C in 5% CO₂. A combined solution of 5 mg/mL MTT/PBS (10 μL/well) was added to each well of the 96-well plate assay, and the cells were incubated for an additional 4 h. Formazan extraction was performed using DMSO, and its quantity was determined colorimetrically using a Synergy H4 Hybrid Microplate reader (BioTek, USA), which measured OD₄₉₀ in nm (absorbance value). The following formula was used to calculate the viability of cell growth: Viability (%) = (mean of absorbance value of treatment group - blank/mean absorbance value of control - blank) × 100.

Calculation of the relaxation rate ($r_1 = 1/T_1$)⁴³. Several parameters can affect the relaxation rate (r_1), which can be calculated by the following equation (1–6):

$$\frac{1}{T_1} = \frac{P_m q}{T_{1m} + \tau_m} \quad (1)$$

where P_m is the mole fraction of metal ion per solvent molecule, q is the number of bound water (or solvent) nuclei per metal ion or the hydration number, τ_m is the average residence time of the solvent molecule in the complex, and T_{1m} is the relaxation times of the bound water molecules.

The relaxation times of the bound water molecules (T_{1m}) are further defined by Solomon-Bloembergen-Morgan (SBM) equations, which represent the sum of dipole-dipole (“through-space”) and scalar (contact or “through-bonds”) contributions:

$$\frac{1}{(T_1)_m} = \frac{1}{T_1^{DD}} + \frac{1}{T_1^{SC}} \quad (2)$$

$$\frac{1}{T_1^{DD}} = \frac{2}{15} \frac{\gamma_1^2 g^2 \mu_B^2 S(S+1)}{r^6} \left[\frac{3\tau_{e1}}{1 + \omega_1^2 \tau_{e1}^2} + \frac{7\tau_{e2}}{1 + \omega_s^2 \tau_{e2}^2} \right] \quad (3)$$

$$\frac{1}{T_1^{SC}} = \frac{2}{3} S(S+1) \left(\frac{A}{\hbar} \right)^2 \frac{\tau_{e2}}{1 + \omega_s^2 \tau_{e2}^2} \quad (4)$$

where γ_1 is the nuclear gyromagnetic ratio; g is the electronic g -factor; μ_B is the Bohr magneton; r is the proton-metal ion distance; ω_1 and ω_s are the proton and electron Larmor precession frequencies, respectively; A/\hbar is the electron-nuclear hyperfine coupling constant; and S is the total electron spin of the metal ion. The dipole-dipole and scalar correlation times, τ_{e1} and τ_{e2} , respectively, that modulate relaxation are defined by

$$\frac{1}{\tau_{e1}} = \frac{1}{T_{1e}} + \frac{1}{\tau_m} + \frac{1}{\tau_R} \quad (5)$$

$$\frac{1}{\tau_{e1}} = \frac{1}{T_{1e}} + \frac{1}{\tau_m} \quad (6)$$

where T_{1e} is the electronic longitudinal and transverse relaxation times of the metal ion, τ_m is the water residence time, and τ_R is the rotational tumbling or correlation time of the entire metal-water complex.

Measurement of relaxivity and MRI. All serum samples were obtained from the College of Public Health, Nantong University, China. Relaxivities were measured on a 0.5 T MR system (Shanghai Niumag Corporation NMI20 Analyst). Peptide 1 and probe 1 were prepared in TBS (pH 7.4, 50.0 mM Tris, 50.0 mM NaCl) at concentrations ranging from 1–100 μM. T_1 was measured using an inversion recovery sequence. The T_1 relaxivities of the agents were calculated from the slopes of the plots of $1/T_1$ versus the concentrations. All samples were measured at 37°C using the internal temperature control of the instrument. T_1 -weighted images at different concentrations in TBS were acquired on a 0.5 T NMI20 analyst using a spin-echo pulse sequence with pulse repetition time $D_0 = 600$ ms.

1. Mayordomo, C. *et al.* Targeting of substance P induces cancer cell death and decreases the steady state of EGFR and Her2. *J. Cell. Physiol.* **227**, 1358–1366 (2012).
2. Felipe, C. D. *et al.* Altered nociception, analgesia and aggression in mice lacking the receptor for substance P. *Nature* **392**, 394–397 (1998).
3. Lucattelli, M., Fineschi, S., Geppetti, P., Gerard, N. P. & Lungarella, G. Neurokinin-1 receptor blockade and murine lung tumorigenesis. *Am. J. Respir. Crit. Care Med.* **174**, 674–683 (2006).
4. Palma, C. Tachykinins and their receptors in human malignancies. *Curr. Drug Targets* **7**, 1043–1052 (2006).
5. Moles, G. *et al.* Cell proliferation associated with actions of the substance P/NK-1 receptor complex in keratocystic odontogenic tumours. *Oral Oncol.* **44**, 1127–1133 (2008).
6. Payan, D. G., McGillis, J. P. & Organist, M. L. Binding characteristics and affinity labeling of protein constituents of the human IM-9 lymphoblast receptor for substance P. *J. Biol. Chem.* **261**, 14321–14329 (1986).
7. Fowler, C. J. & Brännström, G. Substance P enhances forskolin-stimulated cyclic AMP production in human UC11MG astrocytoma cells. *Methods Find. Exp. Clin. Pharmacol.* **16**, 21–28 (1993).
8. Muñoz, M. & Coveñas, R. Involvement of substance P and the NK-1 receptor in cancer progression. *Peptides* **48**, 1–9 (2013).
9. Yuan, Y., Kwok, R. T. K., Tang, B. Z. & Liu, B. Targeted Theranostic Platinum(IV) prodrug with a built-in aggregation-induced emission light-up apoptosis sensor for noninvasive early evaluation of its therapeutic responses in situ. *J. Am. Chem. Soc.* **136**, 2546–2554 (2014).
10. Frank, R. & Hargreaves, R. Clinical biomarkers in drug discovery and development. *Nat. Rev. Drug Discov.* **2**, 566–580 (2003).
11. Zeng, X. *et al.* Lung cancer serum biomarker discovery using glycoprotein capture and liquid chromatography mass spectrometry. *J. Proteome Res.* **9**, 6440–6449 (2010).
12. Mascaux, C. *et al.* Early detection and screening of lung cancer. *Expert. Rev. Mol. Diagn.* **10**, 799–815 (2010).
13. Belinsky, S. A. Gene-promoter hypermethylation as a biomarker in lung cancer. *Nat. Rev. Cancer* **4**, 707–717 (2004).
14. Spira, A. *et al.* Airway epithelial gene expression in the diagnostic evaluation of smokers with suspect lung cancer. *Nat. Med.* **13**, 361–366 (2007).
15. Tan, W., Donovan, M. J. & Jiang, J. Aptamers from cell-based selection for bioanalytical applications. *Chem. Rev.* **113**, 2842–2862 (2013).
16. Liang, H. *et al.* Functional DNA-containing nanomaterials: cellular applications in biosensing, imaging, and targeted therapy. *Acc. Chem. Res.* **47**, 1891–1901 (2014).
17. Zhu, G. *et al.* Noncanonical self-assembly of multifunctional DNA nanoflowers for biomedical applications. *J. Am. Chem. Soc.* **135**, 16438–16445 (2013).
18. Zhao, J., Davidson, M. G., Mahon, M. F., Kociok-Köhn, G. & James, T. D. An enantioselective fluorescent sensor for sugar acids. *J. Am. Chem. Soc.* **126**, 16179–16186 (2004).
19. Wu, J., Zawistowski, A., Ehrmann, M., Yi, T. & Schmuck, C. Peptide functionalized polydiacetylene liposomes act as a fluorescent turn-on sensor for bacterial lipopolysaccharide. *J. Am. Chem. Soc.* **133**, 9720–9723 (2011).
20. Mawn, T. M. *et al.* In vivo detection of phospholipase C by enzyme-activated near-infrared probes. *Bioconjugate Chem.* **22**, 2434–2443 (2011).
21. Ding, D., Li, K., Liu, B. & Tang, B. Z. Bioprobes based on AIE fluorogens. *Acc. Chem. Res.* **46**, 2441–2453 (2013).
22. Alberti, D. *et al.* A Quantitative relaxometric version of the ELISA test for the measurement of cell surface biomarkers. *Angew. Chem., Int. Ed.* **53**, 3488–3491 (2014).
23. Crich, G. *et al.* In vitro and in vivo magnetic resonance detection of tumor cells by targeting glutamine transporters with Gd-based probes. *J. Med. Chem.* **49**, 4926–4936 (2006).
24. Gao, J. *et al.* Ultrasmall near-infrared non-cadmium quantum dots for in vivo tumor imaging. *Small* **6**, 256–261 (2010).



25. Ye, Y. & Chen, X. Integrin targeting for tumor optical imaging. *Theranostics* **1**, 102–126 (2011).
26. Qiu, L. *et al.* A Targeted, self-delivered, and photocontrolled molecular beacon for mRNA detection in living cells. *J. Am. Chem. Soc.* **135**, 12952–12955 (2013).
27. Sheng, W. *et al.* Aptamer-enabled efficient isolation of cancer cells from whole blood using a microfluidic device. *Anal. Chem.* **84**, 4199–4206 (2012).
28. Geninatti Crich, S., Alberti, D., Szabo, I., Aime, S. & Djanashvili, K. MRI visualization of melanoma cells by targeting overexpressed sialic acid with a Gd(III)-dota-en-pba imaging reporter. *Angew. Chem. Int. Ed. Engl.* **52**, 1161–1164 (2013).
29. Sabharanjak, S. & Mayor, S. Folate receptor endocytosis and trafficking. *Adv. Drug Delivery. Rev.* **56**, 1099–1109 (2004).
30. Shaw, S. Y. Molecular imaging in cardiovascular disease: targets and opportunities. *Nat. Rev. Cardiol.* **6**, 569–579 (2009).
31. Zhai, D., Xu, W., Zhang, L. & Chang, Y.-T. The role of ‘disaggregation’ in optical probe development. *Chem. Soc. Rev.* **43**, 2402–2411 (2014).
32. Maggi, C. A. The mammalian tachykinin receptors. *Gen. Pharmacol.* **26**, 911–944 (1995).
33. Pennefather, J. N. *et al.* Tachykinins and tachykinin receptors: a growing family. *Life Sci.* **74**, 1445–1463 (2004).
34. Berton, O. & Nestler, E. J. New approaches to antidepressant drug discovery: beyond monoamines. *Nat. Rev. Neurosci.* **7**, 137–151 (2006).
35. Gröger, G. *et al.* Switchable supramolecular polymers from the self-assembly of a small monomer with two orthogonal binding interactions. *J. Am. Chem. Soc.* **133**, 8961–8971 (2011).
36. Yao, Q.-H., Meng, F.-S., Li, F.-Y., Tian, H. & Huang, C.-H. Photoelectric conversion properties of four novel carboxylated hemicyanine dyes on TiO₂ electrode. *J. Mater. Chem.* **13**, 1048–1053 (2003).
37. Schildkraut, J. S., Penner, T. L., Willand, C. S. & Ulman, A. Absorption and second-harmonic generation of monomer and aggregate hemicyanine dye in Langmuir–Blodgett films. *Opt. Lett.* **13**, 134–136 (1988).
38. Yuan, W. Z. *et al.* Changing the behavior of cChromophores from aggregation-caused quenching to aggregation-induced emission: development of highly efficient light emitters in the solid state. *Adv. Mater.* **22**, 2159–2163 (2010).
39. Hofmeier, H., Hoogenboom, R., Wouters, M. E. & Schubert, U. S. High molecular weight supramolecular polymers containing both terpyridine metal complexes and ureidopyrimidinone quadruple hydrogen-bonding units in the main chain. *J. Am. Chem. Soc.* **127**, 2913–2921 (2005).
40. Kawamoto, S. A. *et al.* Analysis of the interaction of BCL9 with β -catenin and development of fluorescence polarization and surface plasmon resonance binding assays for this interaction. *Biochemistry* **48**, 9534–9541 (2009).
41. Zhang, J. *et al.* Multifunctional envelope-type mesoporous silica nanoparticles for tumor-triggered targeting drug delivery. *J. Am. Chem. Soc.* **135**, 5068–5073 (2013).
42. Yang, L. *et al.* Engineering Polymeric Aptamers for Selective Cytotoxicity. *J. Am. Chem. Soc.* **133**, 13380–13386 (2011).
43. Lauffer, R. B. Paramagnetic metal complexes as water proton relaxation agents for NMR imaging: theory and design. *Chem. Rev.* **87**, 901–927 (1987).
44. Caravan, P. Strategies for increasing the sensitivity of gadolinium based MRI contrast agents. *Chem. Soc. Rev.* **35**, 512 (2006).
45. Bryson, J. M., Reineke, J. W. & Reineke, T. M. Macromolecular imaging agents containing lanthanides: can conceptual promise lead to clinical potential? *Macromolecules* **45**, 8939–8952 (2012).
46. Unger, E. C., Shen, D.-K. & Fritz, T. A. Status of liposomes as MR contrast agents. *J. Magn. Reson. Imaging* **3**, 195–198 (1993).
47. Boros, E., Polasek, M., Zhang, Z. & Caravan, P. Gd (DOTAla): a single amino acid Gd-complex as a modular tool for high relaxivity MR contrast agent development. *J. Am. Chem. Soc.* **134**, 19858–19868 (2012).
48. Hennig, I. M., Laissue, J. A., Horisberger, U. & Reubi, J.-C. Substance-P receptors in human primary neoplasms: Tumoral and vascular localization. *Int. J. Cancer* **61**, 786–792 (1995).
49. Perez, J. M., Josephson, L., O’Loughlin, T., Högemann, D. & Weissleder, R. Magnetic relaxation switches capable of sensing molecular interactions. *Nat. Biotechnol.* **20**, 816–820 (2002).

Acknowledgments

We thank the National Basic Research 973 Program (2013CB733700), the Fundamental Research Funds for the Central Universities (WJ1213007), and the Innovation Program of Shanghai Municipal Education Commission (J100-2-13104) for financial support.

Author contributions

J.W., R.Z. and S.Y. performed the experiments and analyzed data; Y.X., Q.W. and P.W. collected clinical samples; J.W. designed the experiments and supervised the project; J.W. and H.T. wrote the paper.

Additional information

Supplementary information accompanies this paper at <http://www.nature.com/scientificreports>

Competing financial interests: The authors declare no competing financial interests.

How to cite this article: Wu, J. *et al.* A peptide probe for the detection of neurokinin-1 receptor by disaggregation enhanced fluorescence and magnetic resonance signals. *Sci. Rep.* **4**, 6487; DOI:10.1038/srep06487 (2014).



This work is licensed under a Creative Commons Attribution-NonCommercial-NoDerivs 4.0 International License. The images or other third party material in this article are included in the article’s Creative Commons license, unless indicated otherwise in the credit line; if the material is not included under the Creative Commons license, users will need to obtain permission from the license holder in order to reproduce the material. To view a copy of this license, visit <http://creativecommons.org/licenses/by-nc-nd/4.0/>